

## A 33 yr CONSTANCY OF THE X-RAY CORONAE OF AR Lac AND ECLIPSE DIAGNOSIS OF SCALE HEIGHT

JEREMY J. DRAKE<sup>1</sup>, PETER RATZLAFF<sup>1</sup>, VINAY KASHYAP<sup>1</sup>, DAVID P. HUENEMOERDER<sup>2</sup>,  
BRADFORD J. WARGELIN<sup>1</sup>, AND DERON O. PEASE<sup>3</sup>

<sup>1</sup> Harvard-Smithsonian Center for Astrophysics, 60 Garden Street, Cambridge, MA 02138, USA

<sup>2</sup> Massachusetts Institute of Technology, Kavli Institute for Astrophysics and Space Research, 77 Massachusetts Avenue, Cambridge, MA 02139, USA

<sup>3</sup> Space Sciences Laboratory, University of California, Berkeley, 7 Gauss Way, Berkeley, CA 94720, USA

Received 2013 October 17; accepted 2013 December 30; published 2014 February 5

### ABSTRACT

Extensive X-ray and EUV photometric observations of the eclipsing RS CVn system AR Lac were obtained over the years 1997–2013 with the *Chandra X-Ray Observatory Extreme-Ultraviolet Explorer (EUVE)*. During primary eclipse, High Resolution Camera count rates decrease by  $\sim 40\%$ . A similar minimum is seen during one primary eclipse observed by *EUVE* but not in others owing to intrinsic source variability. Little evidence for secondary eclipses is present in either the X-ray or EUV data, reminiscent of earlier X-ray and EUV observations. Primary eclipses allow us to estimate the extent of a spherically symmetric corona on the primary G star of about  $1.3 R_{\odot}$ , or  $0.86 R_{*}$ , and indicate that the G star is likely brighter than the K component by a factor of 2–5. Brightness changes not attributable to eclipses appear to be dominated by stochastic variability and are generally non-repeating. X-ray and EUV light curves cannot therefore be reliably used to reconstruct the spatial distribution of emission assuming that only eclipses and rotational modulation are at work. Moderate flaring is observed, where count rates increase by up to a factor of three above quiescence. Combined with older *ASCA*, *Einstein*, *EXOSAT*, *ROSAT*, and *BeppoSAX* observations, the data show that the level of quiescent coronal emission at X-ray wavelengths has remained remarkably constant over 33 yr, with no sign of variation due to magnetic cycles. Variations in base level X-ray emission seen by *Chandra* over 13 yr are only  $\sim 10\%$ , while variations back to pioneering *Einstein* observations in 1980 amount to a maximum of 45% and more typically about 15%.

**Key words:** binaries: close – stars: activity – stars: coronae – stars: late-type – stars: individual (AR Lac) – X-rays: stars

*Online-only material:* color figures

### 1. INTRODUCTION

AR Lac is the brightest known totally eclipsing system of the RS CVn class of close binaries. RS CVn systems have orbital periods typically between 1 and 14 days, with orbital separations of only a few stellar radii (Hall 1978). Tidal viscosity tends to synchronize the stellar rotation and orbital periods, increasing the rotation rates beyond typical values for all but the youngest single late-type stars. This rapid rotation is thought to engender strong dynamo action that makes them magnetically active and thus copious sources of chromospheric and coronal emission; they are among the very brightest stellar coronal sources observed at short wavelengths with X-ray luminosities up to 10,000 times that of the typical active Sun (e.g., Walter et al. 1978; Pallavicini et al. 1981; Drake et al. 1992; Dempsey et al. 1993; Singh et al. 1996; Makarov 2003; Pandey & Singh 2012).

Only about 1% of the Sun’s surface is covered by bright active region emission during solar maximum (Drake et al. 2000), so even if the entire solar surface were covered in such emission, the RS CVn systems would still be two orders of magnitude more luminous in X-rays. These higher luminosities could be achieved through higher plasma densities, larger radial extent, or a mixture of both. It seems likely that these very active coronae include a continuously flaring component (see also Guedel 1997; Drake et al. 2000). As an eclipsing RS CVn-type system, AR Lac has played a key role in attempts to understand the morphology of these very active stellar coronae.

The first clues to the spatial structure of the AR Lac coronae came from radio observations: Owen & Spangler (1977) failed to detect an eclipse in the quiescent radio emission at 4585 MHz,

a result that suggested that the radio flux originates from a region that is large compared to the radii of the component stars. From radio interferometry, Triguero et al. (2001) determined that the emission was spatially resolved and of order of the binary dimensions; slight variability outside of eclipses suggested modulation by inhomogeneous structures.

Further progress, though with partially conflicting results, was made through direct observations of the hot coronal plasma by the *Einstein* (Walter et al. 1983), *EXOSAT* (White et al. 1990; Siarkowski 1992), *ROSAT* (Ottmann et al. 1993), *ASCA* (White et al. 1994; Siarkowski et al. 1996), *EUVE* (Walter 1996; Christian et al. 1996), and *Beppo-SAX* (Rodonò et al. 1999) observatories. The lack of an obvious eclipse in the harder of two *EXOSAT* X-ray bandpasses led White et al. (1990) to suggest that the hotter and cooler plasma resides in two distinct regions, with the harder emission coming from a much larger region, comparable to the size of the stellar system. This conclusion was bolstered by a similar *EXOSAT* observation showing an apparently uneclipsed hot component on the active binary TY Pyx (Culhane et al. 1990), and fitted well with both the Owen & Spangler (1977) radio result and the finding of Swank et al. (1981) that low-resolution *Einstein* spectra of active stars could be adequately fitted with discrete two-temperature models containing a hard and softer component. Subsequent EUV and X-ray studies all observed distinct primary eclipses,<sup>4</sup> supporting the view that a significant fraction of AR Lac coronal emission must arise from a relatively compact region. Detailed

<sup>4</sup> We adopt here the usual convention for AR Lac designating the G2 IV star to be the primary.

reviews and discussion of these different observations have been presented by Christian et al. (1996) and Rodonò et al. (1999).

Further insights were made spectroscopically, first with *EUVE*, and then with the *Chandra* and *XMM-Newton* observatories, both of which are equipped with diffraction gratings permitting detailed high-resolution spectroscopy in the soft X-ray bandpass (e.g., Weisskopf et al. 2003; den Herder et al. 2001). Griffiths & Jordan (1998) estimated a coronal plasma density of  $5 \times 10^{11} \text{ cm}^{-3}$  based on Fe XXI lines. Huenemoerder et al. (2003) also found tentative evidence for high plasma densities on the order of  $\log n_e \sim 11 \text{ cm}^{-3}$  using lines from the He-like ions of O and Ne formed around  $(2-4) \times 10^6 \text{ K}$ . This result was confirmed by Testa et al. (2004a), who found  $\log n_e = 12.5 \pm 0.5 \text{ cm}^{-3}$  from He-like Mg formed at slightly hotter temperatures of  $\sim 6 \times 10^6 \text{ K}$  (see also Ness et al. 2004). Testa et al. (2004a) also analyzed the *Chandra* spectra of several other active binaries and found similar high densities to generally characterize the coronae of very active stars. High densities point toward compact coronae, though without further spatial diagnostics there remains a degeneracy between surface filling factor and coronal scale height.

The degeneracy was broken for two RS CVn-type binary stars, II Peg and IM Peg, and the active M dwarf EV Lac, which were part of a larger sample whose high-resolution *Chandra* HETG spectra were analyzed by Testa et al. (2004a, 2007). These stars exhibited significant resonance scattering depletion of H-like O and Ne Ly $\alpha$  lines. The size of coronal structures derived from the measured optical depths for all three sources is of the order of a few percent of the stellar radius at most, indicating the presence of compact, dense, and very bright emitting structures.

One drawback of existing X-ray studies of AR Lac is that data generally cover only fractions of an orbit, or concentrate on one orbital period or less. It is difficult to tell from all the disparate observations what the long-term behavior of the source is, how repeatable any eclipses are, and what emission variations are likely to be due to rotational modulation or to simple intrinsic stochastic variability.

The high elliptical orbit of the *Chandra X-Ray Observatory*, combined with high spatial resolution and relatively low noise detectors, provides an advantageous viewpoint for studying the time-dependent X-ray emission of stellar coronae. During on-orbit calibration toward the end of the summer of 1999, AR Lac was favorably placed in the sky and of the right X-ray brightness to make a suitable point-source calibration target for the *Chandra* High Resolution Camera (HRC). As such, it was the first X-ray bright late-type star observed by *Chandra* and has been observed regularly since then to monitor instrument performance. Here we present an analysis of these data that were obtained over a period of 13 yr from 1999 to 2012 and represent the most extensive set of observations of the coronae of AR Lac yet undertaken.

Following a brief summary of the adopted parameters of AR Lac in Section 2, in Section 3 we describe the observational material and data reduction; Sections 4 and 5 present an analysis and discussion of the light curves and their implication for the structure of the AR Lac coronae, as well as the coronae of similarly active stars; a summary and conclusions are presented in Section 7.

## 2. AR Lac

AR Lac lies at a distance of 42 pc (e.g., Siviero et al. 2006), has a period of 1.983 days, and comprises G2 IV and K0 IV stars

**Table 1**  
Relevant Parameters of AR Lac Adopted in This Study (from Popper 1990)

	Primary G2 IV	Secondary K0 IV
Mass	$1.23 M_{\odot}$	$1.27 M_{\odot}$
Radius	$1.52 R_{\odot}$	$2.72 R_{\odot}$
Inclination	$i = 87^{\circ}$	
Primary eclipse <sup>a</sup>	2451745.58650+1.98318608E	

**Note.** <sup>a</sup> From Siviero et al. (2006).

of approximately equal masses but unequal radii, separated by a distance of about  $9.2 R_{\odot}$  (Chambliss 1976; Popper & Ulrich 1977). In the optical band, the G star is completely eclipsed by the K0 subgiant.

We adopt the system parameters of Popper (1990) and the ephemeris of Siviero et al. (2006) that is based on an extensive set of optical eclipse observations. For our purposes, this ephemeris is essentially identical to that of Marino et al. (1998), which was also adopted by Rodonò et al. (1999). The relevant parameters are listed in Table 1. While Lu et al. (2012) have more recently studied the orbital period variation of AR Lac and have produced an analytical formula for the difference between observed and predicted eclipse times (“ $O - C$ ”) relative to the ephemeris of Siviero et al. (2006), these  $O - C$  corrections do not seem to match the data of Siviero et al., with values of  $O - C$  close to 0.1 days for the range of epochs on which Siviero et al. base their ephemeris. We also find that the *EUVE* and *Chandra* eclipses reported here are not consistent with the Lu et al. (2012)  $O - C$  values.

## 3. OBSERVATIONS AND LIGHT CURVES

### 3.1. *Chandra* X-Ray Photometry

Regular *Chandra* observations of AR Lac have been performed using the HRC imaging and spectroscopic (HRC-I, HRC-S) detectors since the initial on-orbit calibration phase in 1999. These data were obtained for the purposes of verifying the focus and imaging performance of the combined mirror and detector assembly. The HRC instrument is of microchannel plate design, with sensitivity in the 0.07–10 keV range and peaking around 1 keV, and provides photon timing resolution of a few ms in the standard mode employed for the data presented here (and up to  $16 \mu\text{s}$  in a special “timing mode”; Kenter et al. 2000) that enable accurate light curves to be constructed. Since the detectors themselves have only very low energy resolution, no attempt was made to constrain or filter detected events in energy.

The AR Lac observations were aimed at different off-axis angles to obtain pointings over a range of detector locations in a coarse “raster,” with each pointing typically lasting from one to a few ks. Each pointing has associated “start” and “stop” times separated by short intervals during which the detector high voltage was ramped down. The observations are summarized in Table 2, though details of the individual pointings within each visit are omitted. In a small handful of cases, individual pointings were found to have dithered onto the High Energy Suppression Filter attached to the HRC-S and were discarded.

Satellite telemetry was processed by standard *Chandra* X-ray Center (CXC) pipeline procedures to produce photon event lists. Raw instrument count rates were examined to ensure that the data were not affected by telemetry saturation, which can lead to significant deadtime. Times of telemetry saturation and where

**Table 2**  
*Chandra* HRC Observations of AR Lac Used in This Analysis

Observation ID	Detector	UT First Start	UT Last Stop	Elapsed (ks)	Exposure (ks)
1283–1289, 1294–1295	I	1999-08-31T19:31:51	1999-09-01T00:41:32	19	7
1319–1382, 1385	I	1999-10-03T13:10:26	1999-10-05T05:34:48	145	103
1484–1504	I	1999-12-09T09:41:42	1999-12-09T20:40:04	40	25
996, 2345–2364	I	2000-12-12T16:31:38	2000-12-13T01:37:11	33	25
998, 2366–2385	S	2000-12-20T14:52:41	2000-12-20T23:51:27	32	24
997, 2432–2451	S	2001-05-14T00:05:25	2001-05-14T10:30:09	37	28
2625–2645	S	2002-01-26T14:09:49	2002-01-26T23:03:17	32	24
2604–2624	I	2002-01-26T23:03:17	2002-01-27T08:01:37	32	25
2646–2666	S	2002-08-09T11:30:11	2002-08-10T12:52:59	91	18
4332–4352	S	2003-02-22T00:26:08	2003-02-22T09:26:05	32	24
4290–4310	I	2003-02-22T09:26:05	2003-02-22T18:23:36	32	24
4311–4331	S	2003-09-01T09:42:51	2003-09-01T18:59:46	33	23
5081–5101	S	2004-02-09T12:59:22	2004-02-09T21:39:16	31	22
5060–5062	I	2004-09-13T20:19:58	2004-09-13T21:39:48	5	3
5063–5080, 6133–6135	I	2004-11-25T13:40:27	2004-11-25T22:21:40	31	22
5102–5122	S	2004-11-28T05:42:35	2004-11-28T14:13:21	31	22
6021–6041	S	2005-02-10T10:38:01	2005-02-10T20:24:24	35	26
6000–6020	S	2005-09-01T20:58:49	2005-09-02T06:40:12	35	26
5979–5989	I	2005-09-27T08:06:24	2005-09-27T13:38:26	20	7
5996–5997	I	2005-10-02T19:10:59	2005-10-02T20:12:35	4	2
5990–5992	I	2005-10-09T14:54:37	2005-10-09T16:47:07	7	2
5993–5995, 5998–5999	I	2005-10-17T18:19:18	2005-10-17T23:35:24	19	6
6477–6497	S	2006-03-20T05:05:39	2006-03-20T15:02:41	36	26
6519–6539	I	2006-09-20T19:20:57	2006-09-21T05:06:40	35	27
6498–6518	S	2006-09-21T18:56:18	2006-09-22T04:51:09	36	26
8298–8318	I	2007-09-17T13:08:38	2007-09-17T22:40:41	34	27
8320–8340	S	2007-09-21T17:06:23	2007-09-22T03:05:09	36	26
9682–9683	S	2008-07-11T07:47:29	2008-07-11T09:55:09	8	6
9684–9685	I	2008-07-11T09:55:09	2008-07-11T11:53:54	7	6
9661–9681	S	2008-09-02T02:37:56	2008-09-02T13:31:27	39	30
9640–9660	I	2008-09-07T09:35:46	2008-09-07T20:03:22	38	30
10578–10598	I	2009-09-24T16:07:52	2009-09-25T01:53:30	35	26
10601–10621	S	2009-09-25T21:51:14	2009-09-26T07:35:29	35	27
11889–11909	I	2010-09-25T02:40:08	2010-09-25T12:09:40	34	27
11910–11930	S	2010-09-25T12:09:40	2010-09-25T21:42:13	34	26
13182	I	2010-12-16T18:45:33	2010-12-17T00:14:08	20	18
13265, 13048–13067	I	2011-09-18T20:48:16	2011-09-19T06:06:52	34	26
13068–13088	S	2011-09-19T06:06:52	2011-09-19T15:49:50	35	26
14278–14298	S	2012-09-24T09:42:17	2012-09-24T19:23:23	35	26
14299–14319	I	2012-09-27T02:28:47	2012-09-27T12:14:25	35	27
15409–15429	I	2013-09-16T15:20:29	2013-09-18T06:39:54	142	27
15430–15450	S	2013-09-16T18:11:51	2013-09-18T08:31:45	138	26

the instrument dead time might be significant (as judged by the flag  $DTF < 0.98$ ) were discarded.

Data analysis employed standard CIAO v4.5 procedures and calibration database CALDB v4.5.5. The event files were partitioned into 400 s bins (and whatever exposure remained in the final bin). For each bin, spectrum-weighted exposure maps, describing the product of effective area and exposure time, of the detector region under the dithered source region were generated using standard CIAO tools. The weighting spectrum was computed using the APEC model in XSPEC, using four discrete components normalized to match the emission measure distribution as a function of temperature of Huenemoerder et al. (2003). We emphasize that the exact choice of spectral parameters is not important here (see also Section 6). Net source counts were extracted from circular source regions whose radii depended on off-axis angle and surrounding background annulus regions. Energy and photon fluxes were then calculated by dividing the net counts by the exposure map value in the appropriate units of the pixel at the center of the source region.

**Table 3**  
*EUVE* Observations of AR Lac Analyzed Here

UT Start	UT Stop	Exposure (s)
1997-07-03 13:40:17	1997-07-06 06:25:48	84758
2000-09-04 05:46:34	2000-09-08 10:12:25	137359
2000-09-08 11:08:44	2000-09-12 15:31:02	132807
2000-09-14 16:47:33	2000-09-18 00:56:34	79949

A composite of all the *Chandra* HRC-I and HRC-S observations is illustrated as a function of orbital phase in Figure 1.

### 3.2. *EUVE* Observations

AR Lac was observed with the *EUVE* Deep Survey (DS) telescope on four separate epochs, one in 1997 July and three in 2000 September, for a total exposure time of 435 ks. Details of the observation times are listed in Table 3. Photons

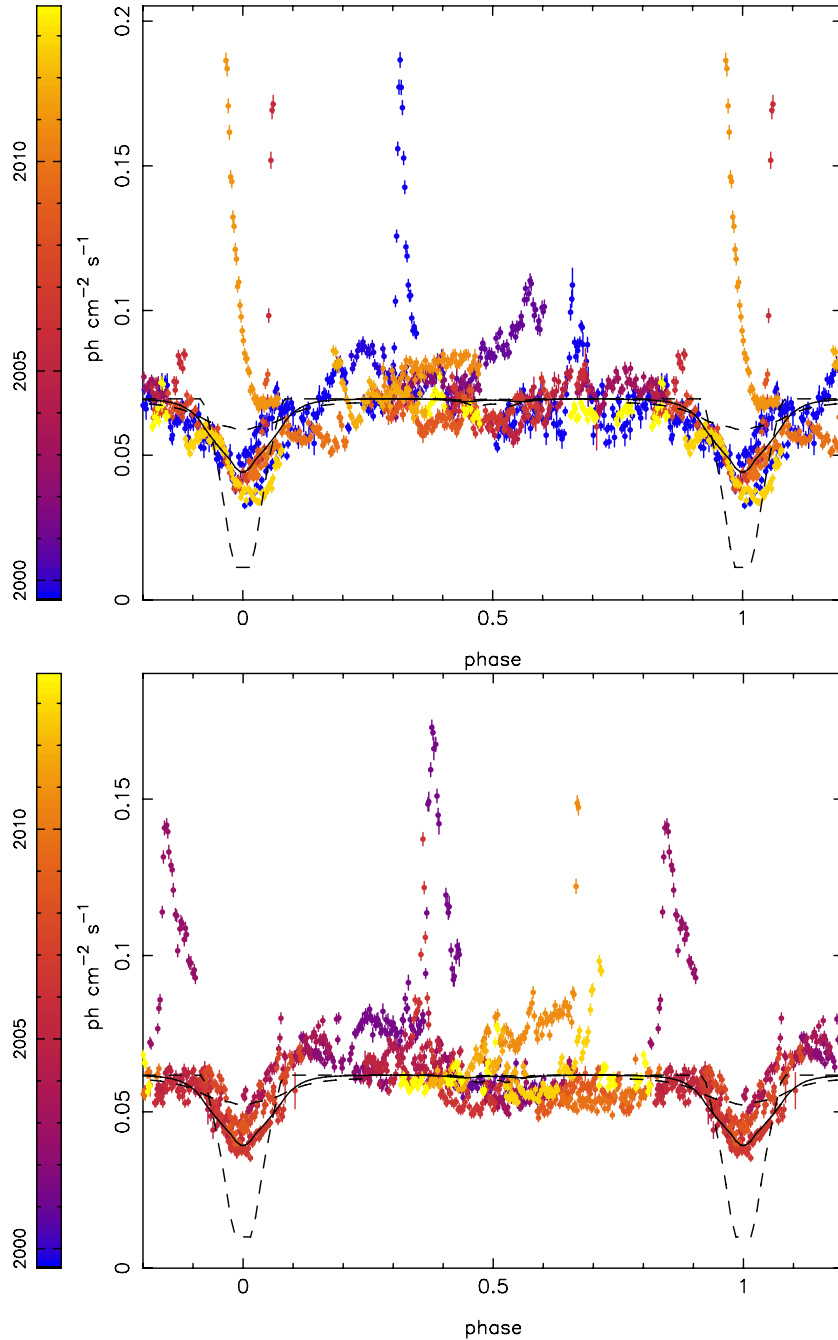


**Figure 1.** Phased composite HRC-I (top) and HRC-S (bottom) X-ray light curves of AR Lac for all the epochs listed in Table 2. Data are color-coded according to the time of acquisition and are compared with model light curves for spherically symmetric coronae on both components. Models, from top to bottom, are for coronal scale heights of 0.2, 0.5, and  $1.0 R_{\odot}$ .

(A color version of this figure is available in the online journal.)

gathered by the DS telescope either are intercepted by three symmetrically oriented grazing incidence diffraction gratings, or else pass through to the DS detector. On-axis photons, such as would be observed from a point source during a normal spectroscopic pointing, fall on a boron-coated Lexan filter supported on a nickel mesh, having significant transmission between approximately 65 and 190 Å and peaking near 90 Å with an effective area of about 28 cm<sup>2</sup>. A complete description of the *EUVE* instrument and its performance can be found in Welsh et al. (1989) and Bowyer & Malina (1991). The sensitivity of the *EUVE* instruments in terms of optically thin plasma emission,

as is expected to characterize the coronae of active stars like AR Lac, has been thoroughly discussed by Drake (1999).

We obtained DS QPOE (quick position-ordered event) files from the *EUVE* archive and processed the data using the most current telescope effective area, vignetting corrections, and “Primbs” corrections for when the telemetry was busy. We obtained the DS light curve using the standard *EUVE* IRAF software. Light curves for the separate *EUVE* observations binned at 1000 s intervals are illustrated in Figure 2. A flare amounting to a peak count rate of 10 times the quiescent value was detected in the last observational segment; this is illustrated

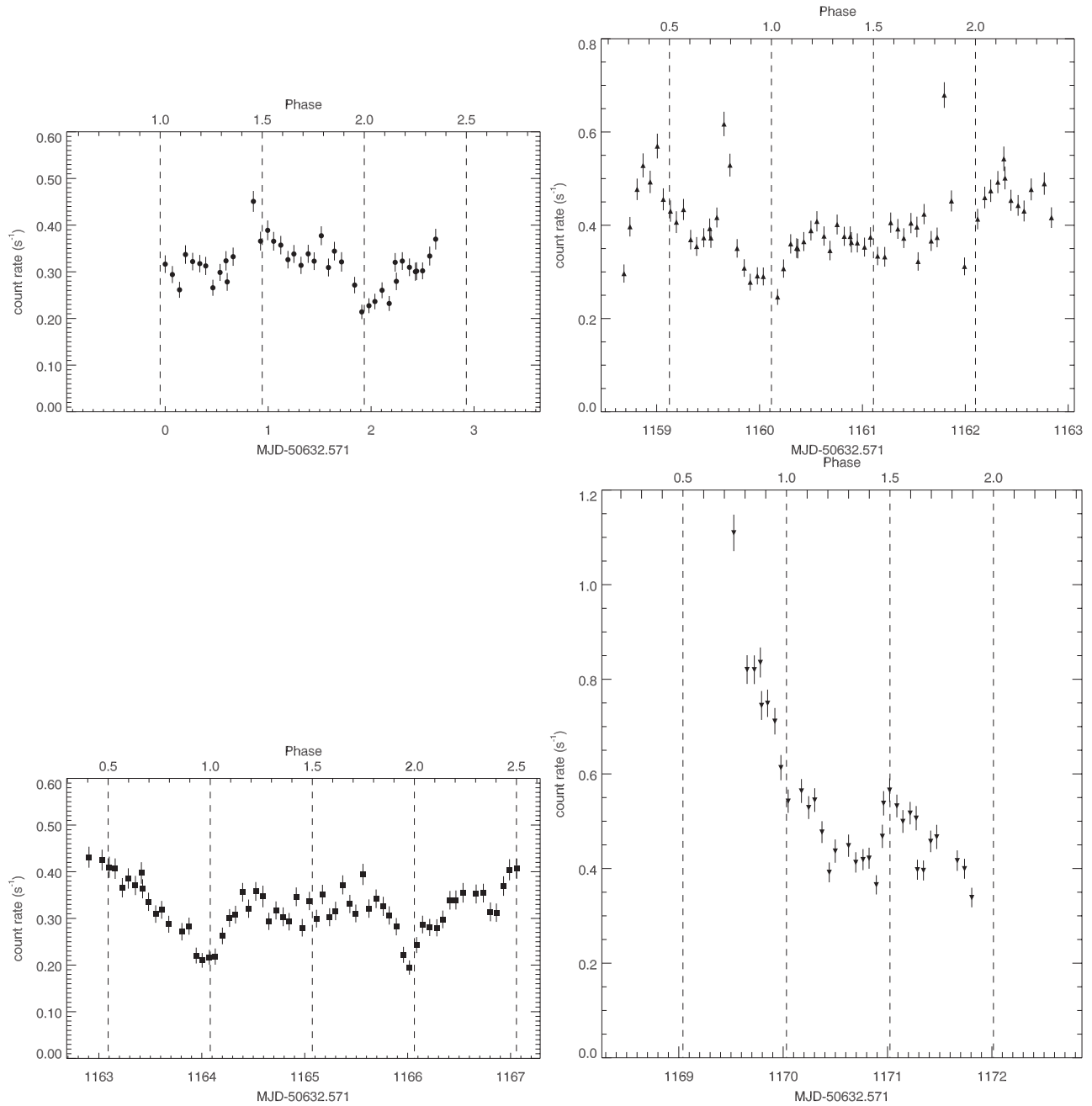


**Figure 2.** *EUVE* light curves for the four epochs analyzed here. Data are binned on 1000 s intervals. Each panel is sized such that the y-axis scale is the same for all, and the bottom panel does not include the flare peak at about 4.6 counts  $s^{-1}$ ; see Figure 3 for the full detail.

in Figure 3. The data are illustrated as a function of orbital phase in Figure 4.

#### 4. LIGHT-CURVE ANALYSIS

Both *Chandra* and *EUVE* sets of light curves are characterized by stochastic variability and flaring, but also by prominent primary eclipses in the majority of epochs in which the eclipse was covered. There are no obvious signs of the secondary eclipse in either the X-ray or EUV data; we will return to this in the discussion below.

##### 4.1. Constraining the Coronal Scale Height

The simplest coronal model to consider is a spherically symmetric shell of emission surrounding both stars that is constant

in time. Such a model has a well-behaved, symmetrical primary eclipse whose width and depth depend on the relative brightness of the two stars and the coronal scale height. Unfortunately, Figure 8 demonstrates that “clean” and perfectly symmetrical coronal primary eclipses that can easily be interpreted in terms of spherical emitting geometry are fairly rare. However, there are a number of primary eclipses in which ingress or egress does appear to follow the shape expected for such a spherical shell of emission and that are unaffected by significant flares. We have extracted these and have fitted a coronal emission model.

Our model comprises a numerical spherically symmetric intensity profile exponentially decaying with height placed on each star. These intensity profiles are placed in a three-dimensional Cartesian system, and the intensities are projected onto a plane perpendicular to the direction of observation. The

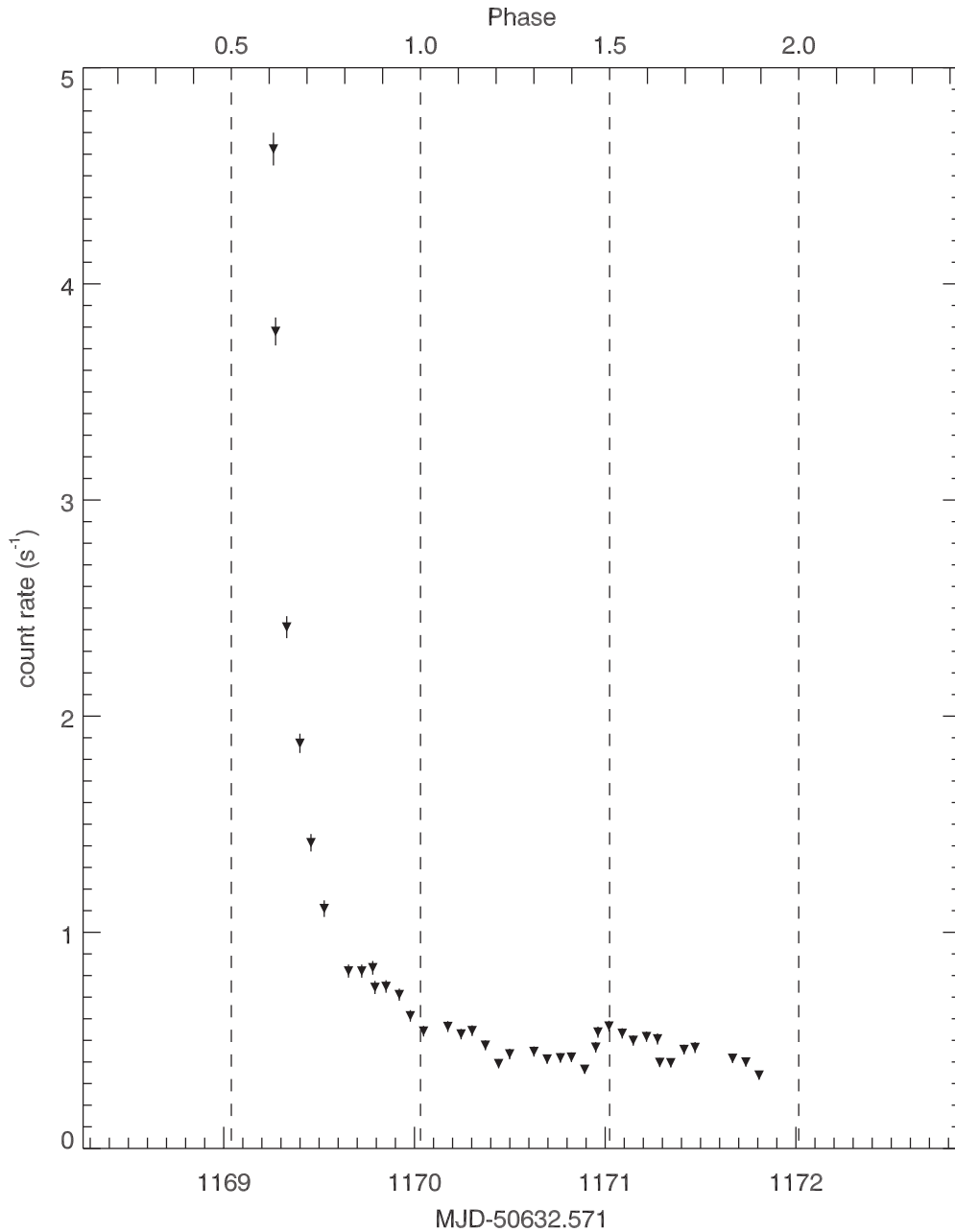
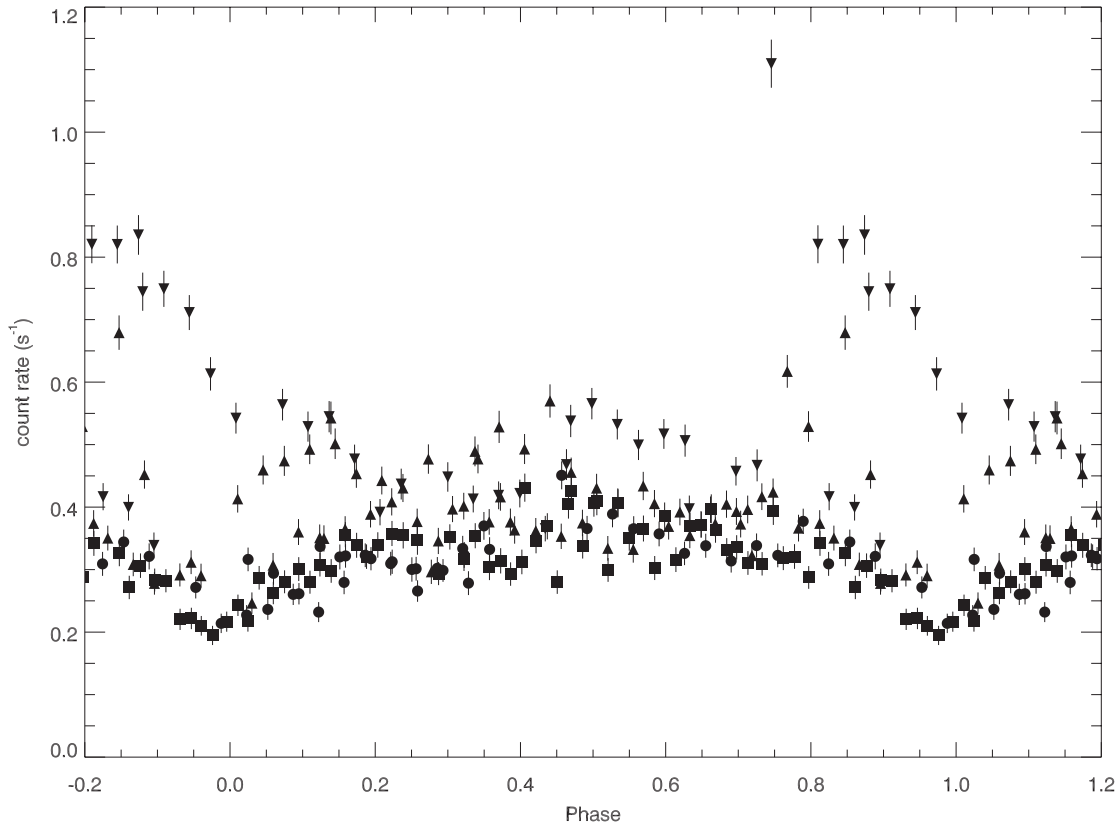


Figure 3. Detail of the flare detected by *EUVE* on 2000 September 14.

disks of the stars are opaque, and the atmospheres are assumed to be fully transparent such that neither primary nor secondary corona contributes to any dimming of the corona behind it. Using the system parameters listed in Table 1, we compute the projected coronal emission as a function of orbital phase and produce artificial light curves. There are three free parameters: the K star is characterized by a scale height  $h_K$  and relative brightness  $b_K$ , and the secondary G star has a scale height  $h_G$  and a fixed brightness  $b_G = 1$ . The overall normalization of the model is set separately for each data set to be the median count rate of all rates for a given instrument over the phase range 0.15–0.85. These values were found to be 0.074, 0.064, and 0.33 photons  $s^{-1} cm^{-2}$  for *Chandra*/HRC-I, *Chandra*/HRC-S, and *EUVE*/DS, respectively. An image of the modeling approach for typical parameters for AR Lac is illustrated in Figure 5, and illustrative model curves for different parameter values are shown in Figure 6.

Figure 6 illustrates the comparative lack of sensitivity of the eclipses to the scale height of the corona of the larger K star, even for the case in which this component is brighter than the G star. The secondary eclipse depth, when the G star is in front, changes by only 10% or so for K star scale height changes of a factor of 10 or more. We fail to detect the secondary eclipse unambiguously in any of our observations, and therefore we concentrate on the analysis of primary eclipse and the G star coronal scale height.

We performed a brute-force grid search of the model parameters for the best fit to the observations over phases  $\pm 0.15$  around the primary eclipse with the K star in front. This was done for the different cases of HRC-I, HRC-S, and *EUVE* data treated both separately and with all data combined. For the combined data, fitting was also performed for ingress and egress separately. The  $\chi^2$  values are calculated assuming both a statistical error ( $\propto \sqrt{\text{counts}}$ ) and a nominal 10% excess



**Figure 4.** *EUVE* light curves for all four epochs shown as a function of orbital phase. Plot symbols correspond to those in Figure 2 for the four epochs analyzed here. Data are binned on 1000 s intervals.

error attributable to intrinsic variability. The likelihood of seeing the observed data,  $D$ , given the model is then computed as  $p(D|h_K, h_G, b_K) = e^{-\chi(h_K, h_G, b_K)^2/2}$ . We adopt flat priors on all parameters over the grid range and multiply them with the likelihood. Following Bayes' theorem, this generates the joint posterior probability density distribution of the parameters given the data,

$$p(h_K, h_G, b_K|D) \propto p(h_K)p(h_G)p(b_K)p(D|h_K, h_G, b_K). \quad (1)$$

We then obtain posterior density distributions for each parameter by marginalizing over the other two,

$$p(h_K|D) \propto \int dh_G db_K p(h_K, h_G, b_K|D), \quad (2)$$

$$p(h_G|D) \propto \int dh_K db_K p(h_K, h_G, b_K|D), \quad (3)$$

$$p(b_K|D) \propto \int dh_K dh_G p(h_K, h_G, b_K|D), \quad (4)$$

although in practice we have no information to usefully constrain the scale height of the K star corona,  $h_K$ . The modes of the distribution correspond to locations of minimum  $\chi^2$ . These and the 68% half-tail credible regions are reported in Table 4. The model curves for the best-fit values obtained by jointly fitting all data sets (excluding periods of obvious flares) are shown in Figure 7. The fits are also shown in Figure 8 for primary eclipses observed by the *Chandra* HRC that are uncontaminated by obvious flaring.

The best-fit model parameters generally indicate that the G star corona has a scale height of about 1.3 solar radii and is

**Table 4**  
Model Parameter Estimates

Data Set		$h_G$ ( $R_\odot$ )	$b_K$	$\chi^2/\nu$
Full eclipse	HRC-I	$1.3^{<1.33}_{>1.27}$	$0.20^{<0.22}_{>0.20}$	571/389
Full eclipse	HRC-S	$0.7^{<0.74}_{>0.68}$	$1.16^{<1.16}_{>1.15}$	344/330
Full eclipse	<i>EUVE</i>	$1.5^{<1.59}_{>1.46}$	$0.20^{<0.3}_{>0.2}$	79/80
Full eclipse	<i>EUVE</i> + HRC-I + HRC-S	$1.3^{<1.36}_{>1.27}$	$0.44^{<0.48}_{>0.40}$	1357/802
Ingress	<i>EUVE</i> + HRC-I + HRC-S	$1.25^{<1.33}_{>1.20}$	$0.53^{<0.60}_{>0.49}$	352/358
Egress	<i>EUVE</i> + HRC-I + HRC-S	$1.4^{<1.44}_{>1.36}$	$0.29^{<0.38}_{>0.26}$	998/366

brighter than that of the K star by a factor of 2–5. The fit parameters for HRC-I and *EUVE* are reasonably consistent with one another, while the best-fit HRC-S scale height is a factor of two smaller and the relative brightness parameter,  $b_K \sim 1$ , suggests that both stars are of approximately equal brightness. However, visual inspection of the data and models in Figure 7 reveals substantial deviations between them, particularly at egress. This will be discussed further in Section 5 below.

The results for ingress and egress treated separately are generally consistent for the values of coronal scale height, within the uncertainties of the measurements. The relative brightness parameter is marginally different though, with a best-fit value slightly larger by about 40% for ingress than egress.

#### 4.2. Flares

Both *Chandra* and *EUVE* observations are characterized by a number of flares. The *Chandra* flares could all be described as fairly modest, with the largest having peaks only a factor of three or so higher than the quiescent level, and decay timescales

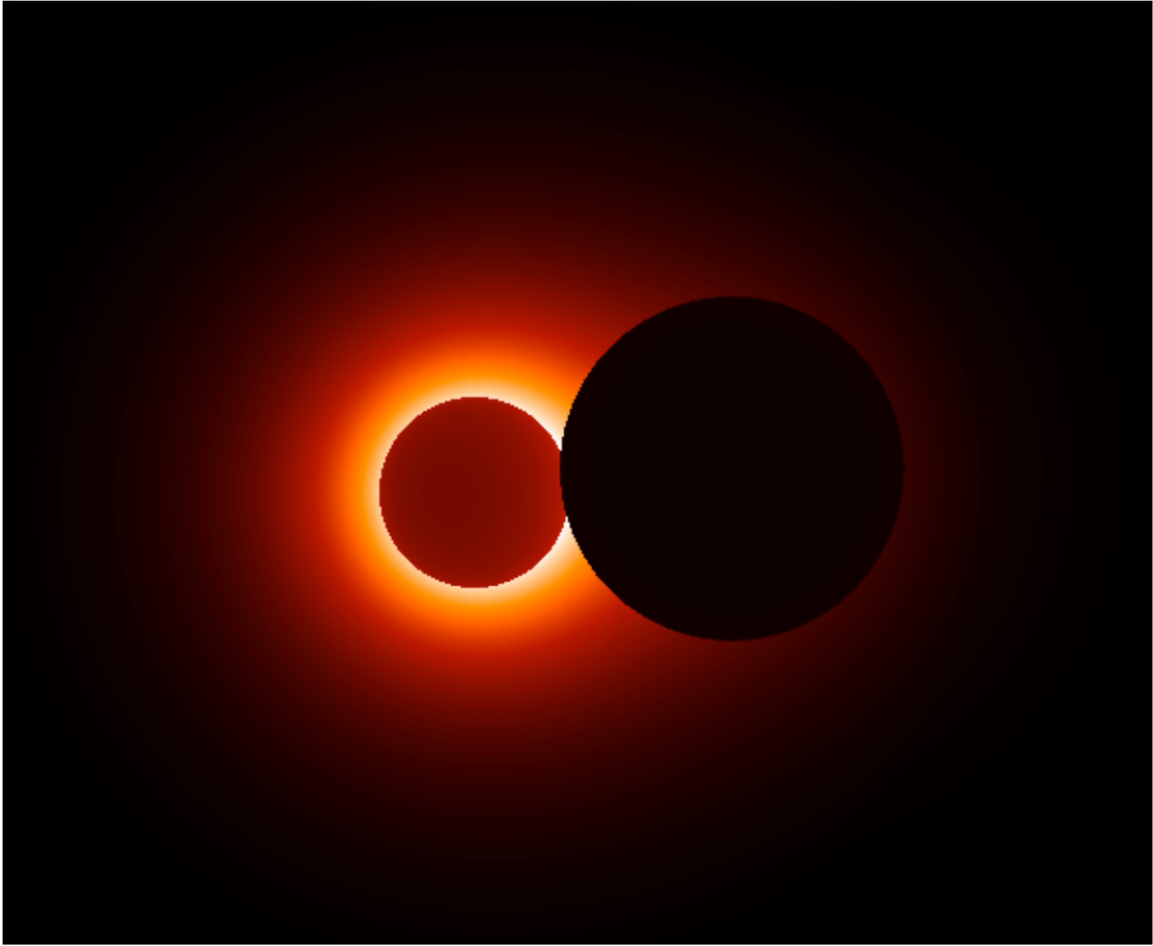


**Figure 5.** Illustration of the spherically symmetric coronal model as the stars approach primary eclipse with the larger K star in front. Each star is assumed to be opaque and surrounded by a transparent spherical shell of emission with an exponential decline with height. The model shown corresponds to the parameters  $h_K = h_G = 1.3 R_\odot$  and  $b_K = 0.44$ .

(A color version of this figure is available in the online journal.)

of a few ks. A full analysis of this flaring component is beyond the scope of this paper. The last *EUVE* epoch that began on 2000 September 14, however, happened upon a large event whose rise phase occurred before the observation start, but whose decay was tracked over two days (see Figure 3). The spectrum of the event was previously analyzed by Sanz-Forcada et al. (2003), who reported a flare fluence of  $2.0 \times 10^{35}$  erg.

To refine the flare characteristics, we fitted the *EUVE* light curve of this large flare using Weibull distributions following the method described in detail by Huenemoerder et al. (2010). This normalized distribution is defined by the equations

$$f(p, a, s) = \left(\frac{a}{s}\right) p^{(a-1)} e^{-p^a}, \quad (5)$$

$$p = (t - t_0)/s, \quad (6)$$

where  $a$  is a shape parameter and takes values  $a > 0$ ,  $s$  describes the scale or width of the distribution and is also positive,  $s > 0$ , and  $t$  is the time coordinate with the time of flare onset given by  $t_0$ . An amplitude parameter normalizes to the total counts, and we included a constant term as an estimate of the quiescent rate. While this is an empirical parameterization of a flare, the function can range from purely exponential form for  $a = 1$ , to steeper for  $a < 1$ , or shallower for  $a > 1$ , to smooth rise and decay for large  $a$ .

We fitted both the large flare and a smaller event that occurred nearly 2 days after the observation start. The free parameters in the model are the normalization factor,  $a$ ,  $s$ , and  $t_0$ , and the best fit is illustrated in Figure 9. The large flare contains 66,000 counts and a scale of 25 ks and is slightly steeper than exponential ( $a = 0.82$ ), while there are 4700 counts in the smaller flare, offset by 146 ks, the same scale, but slightly slower than exponential ( $a = 1.2$ ). The constant term had a value of  $0.37 \text{ counts s}^{-1}$ .

To estimate the flare energy, we used two methods. First, the scaling relations between observed counts and source flux for an isothermal spectrum with a flare-like temperature of  $2 \times 10^7$  K given by Drake (1999, Table 8) indicate that one count in the *EUVE* DS Lex/B filter corresponds to an energy of about  $3 \times 10^{-11} (2\pi D^2)$  erg, in the 65–195 Å bandpass, for a distance  $D$ . Here, we used an interstellar absorption column density of  $N_H = 2 \times 10^{18} \text{ cm}^{-2}$  derived by Walter (1996) based on *EUVE* spectra of AR Lac, which is similar to the value derived by Sanz-Forcada et al. (2003). Since a flare is thought to arise on a fairly discrete, limited part of the corona, we have also divided the flux from Drake (1999) by two to remove the correction factor introduced to account for the “unseen” corona on the far side of the star (see, e.g., Jordan et al. 1987). For a total of 66,000 counts, we find an EUV fluence of  $2.1 \times 10^{35}$  erg.

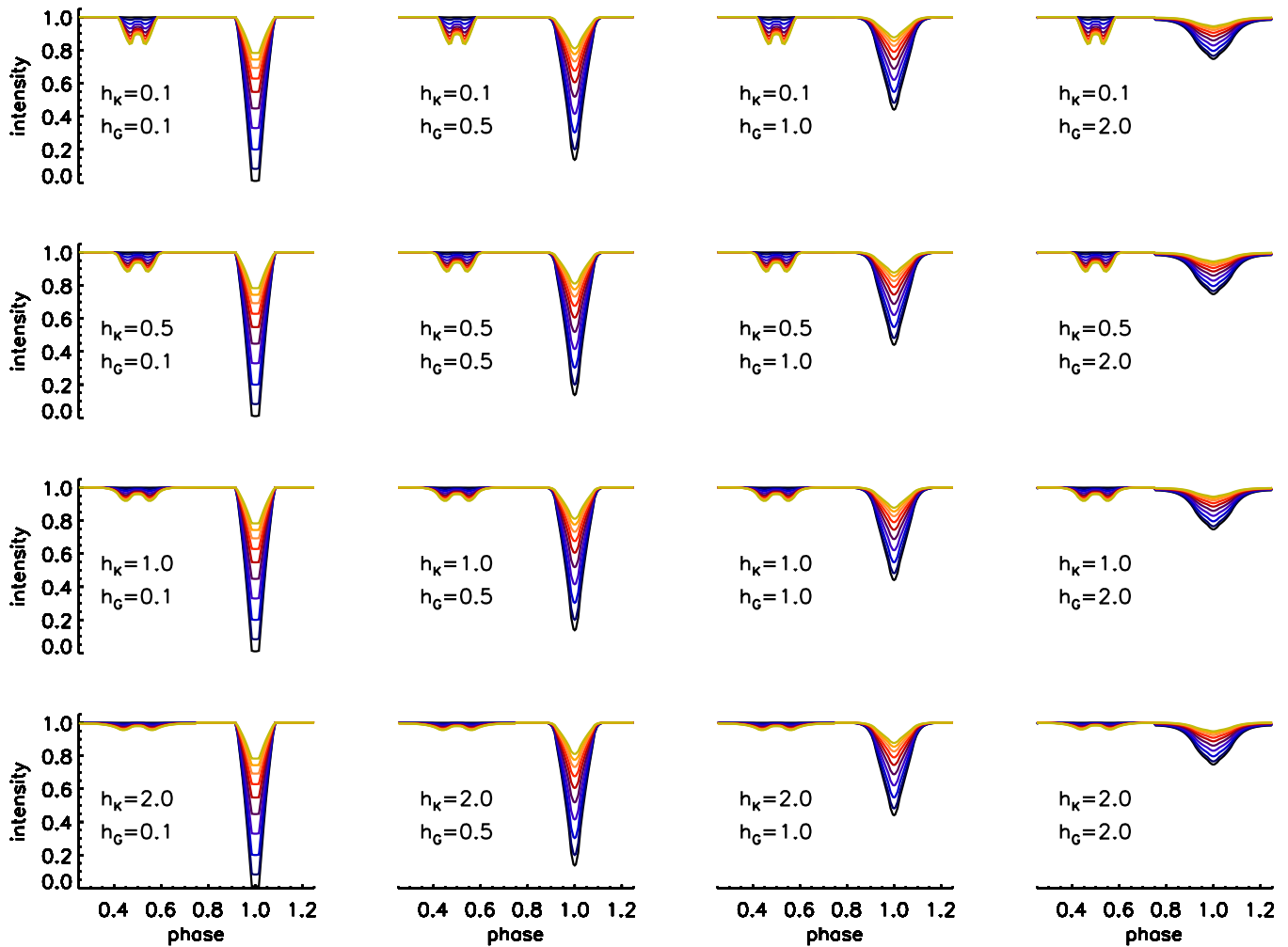


**Figure 6.** Illustration of how the primary and secondary eclipse profiles change with the free parameters in the light-curve model:  $b_K$ ,  $h_K$ , and  $h_G$ ;  $b_G$  is normalized to 1 for all models. The parameter  $h_K$  increases from top to bottom and is fixed from left to right. Conversely,  $h_G$  increases from left to right and is held fixed from top to bottom. The measure of the relative brightness of the primary and secondary coronae,  $b_K$  (with  $b_G$  being normalized to 1), goes from 0.1 (blue; dark) to 2.0 (yellow; light) in steps of 0.3.

(A color version of this figure is available in the online journal.)

Second, we adopted the plasma model (emission measure distribution (EMD) and elemental abundances) of Huenemoerder et al. (2003) derived from HETG spectra obtained around the same time as the *EUVE* data, between 2000 September 11 and 19. However, we found their normalization too high and had to rescale the model to an integrated emission measure of  $4.9 \times 10^{53} \text{ cm}^{-3}$  to better match the X-ray spectrum of the approximately steady flux of *Chandra* Observation ID 9. This EMD also closely matches that derived by Sanz-Forcada et al. (2003) from the *EUVE* flare spectrum. As such, it represents some mean of flare and quiescent plasma EMDs.

For this model and a distance of 42 pc, the EUV flare photons (in the range of 65–190 Å) represent a fluence of  $1.8 \times 10^{35}$  erg (a lower limit since the flare onset was not observed), in good agreement with both Sanz-Forcada et al. (2003) and the estimate based on the Drake (1999) tables. Scaling this to the HETG band (1.7–25 Å) would produce an X-ray flare fluence of  $1.3 \times 10^{36}$  erg, indicating that the radiative output of the hot flare plasma is dominated by X-ray emission.

While the flare looks very large in the EUV, the estimated X-ray flare fluence is typical for large flares of young active stars, which have a similar activity level as RS CVn binaries (see, e.g., Schulz et al. 2006, Figure 7).

## 5. DISCUSSION

Eclipse observations provide potentially powerful diagnostics of the geometry of the emitting regions and have provided the main motivation for studies of the outer atmospheres and coronae of the AR Lac system. Figures 1 and 4, however, starkly illustrate the difficulties in interpreting such data in terms of obscuration and rotational modulation. The X-ray and EUV source flux is in a state of frequent change on a variety of timescales, and it is often unclear whether these variations are due to geometrical effects or simply reflect stochastic brightening and dimming of the emitting regions. Clear rotationally modulated variations in coronal EUV and X-ray emission of active stars have often been sought after and occasionally seen but are not common and even when identified tend to account only for a fraction of the observed variations (see, e.g., Agrawal & Vaidya 1988; Drake et al. 1994; Guedel et al. 1995a, 1995b; Kuerster et al. 1997; Audard et al. 2001; García-Alvarez et al. 2003; Marino et al. 2003; Flaccomio et al. 2005). Attempts at geometrical reconstruction of the emitting regions based on limited coverage, or only a single rotation phase, in which all variations are assumed to arise from rotational modulation, are then very likely to result in spurious structure.

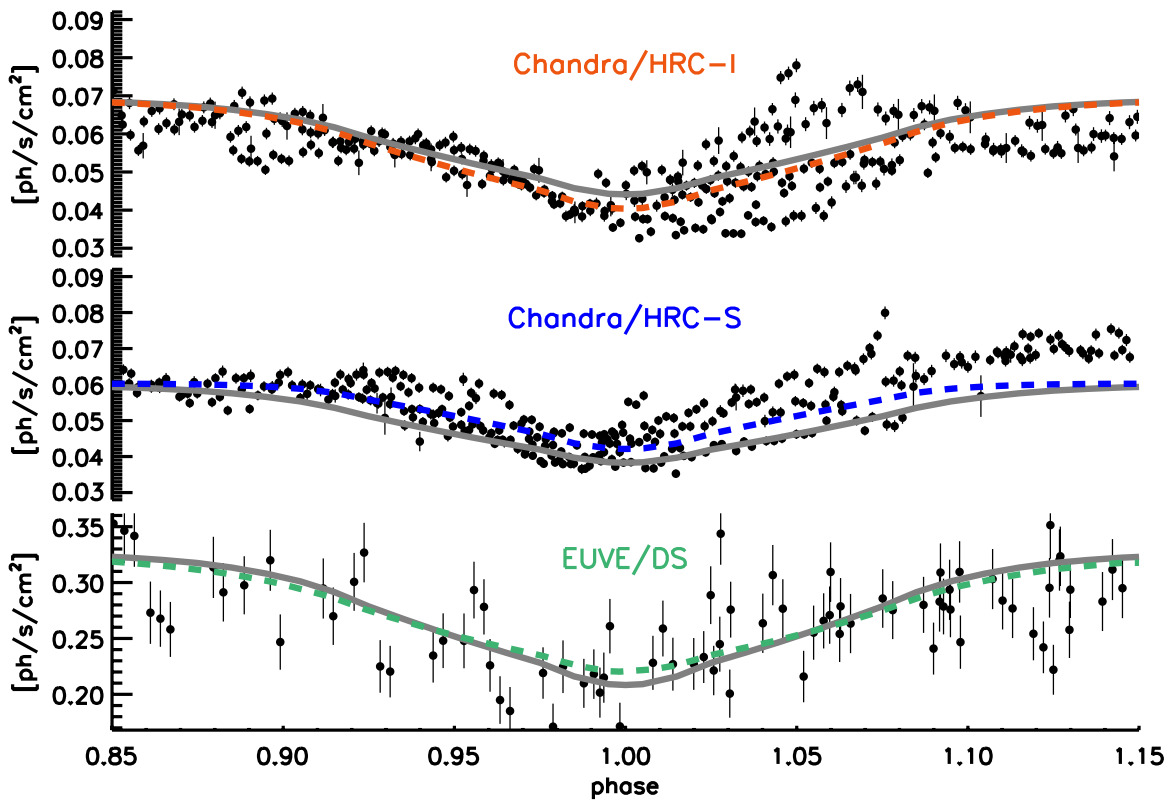


**Figure 7.** Illustration of the best-fit light-curve model overlaid with the *Chandra* HRC and *EUVE* data as a function of orbital phase. Best fits to all the data combined (gray) and to the individual data sets (colored) are shown. The best-fit parameters are listed in Table 4. (A color version of this figure is available in the online journal.)

### 5.1. Coronal Scale Height and Substructure

The light-curve modeling described in Section 4.1 at face value succeeded in constraining the coronal scale height of the G-type primary but not that of the K-type secondary star. There are three issues to consider in interpreting the results. First, while it appears that simple, spherically symmetric models with only three free parameters are capable of providing a reasonably good match to the observed light curves, a quasi-infinite range of models of increased complexity and asymmetry could be constructed that could match the observations equally well (or hopefully better, given more free parameters). Second, the observed eclipses do not all have the same profile and can differ quite significantly between epochs. This is evident from the *EUVE* phased light curve illustrated in Figure 4, but is graphically illustrated in Figure 8, showing sequentially the *Chandra* eclipses that are unaffected by flaring. While some portions of the data follow the best-fit eclipse model quite well, such as epochs 2005.67 and the first half of the eclipse of epoch 1999.76, this is the exception rather than the norm. Third, the model assumes that the emission is effectively constant throughout the eclipse, an assumption that is rendered catastrophically inappropriate during flares, but that also might be questioned during relative quiescence. We can assess the latter to some extent by examination of the light curves out of eclipse near quadrature phases, when only rotational modulation is otherwise at work.

The *EUVE* observations covering more than one orbital phase in Figure 2 demonstrate that brightness as a function of orbital phase is not very repeatable. On shorter timescales, the non-flaring data are mixed in terms of variability. There are periods

of stability with little variation, such as in the HRC-S data illustrated in Figure 1 between phases 0.6 and 0.9, yet there are also a lot of brightenings and dimmings at other times, such as in the HRC-I data at phases 0.1–0.4. Asymmetries in Mg II line profiles associated with active regions on the K component were detected by Pagano et al. (2001), and it is likely that some of the eclipse asymmetries and other secular variations on orbital timescales observed here are a coronal signature of analogous active regions. Pagano et al. (2001) also noted, however, that emission on the G component appeared more uniform. Small variations might also be caused by absorbing material in the line of sight, as suggested by Walter (1996) based on EUV observations and inferred from the UV study of Pagano et al. (2001). In the former case, Walter (1996) estimated that an equivalent absorbing column,  $n_H$ , of only  $10^{19} \text{ cm}^{-2}$  would be required, which would likely not have a noticeable effect on the higher energy X-rays observed in this study.

There is a limit to how much the non-flare variations can be caused by simple rotational modulation while still providing eclipses that follow to a reasonable degree what would be expected from a spherically distributed corona. A compact bright active region hoving into view around the limb, for example, can cause a fairly rapid brightening, but would also cause a sharp drop as it was obscured during an eclipse. It seems more likely that the most rapid variations observed are largely changes in brightness of visible regions in the coronae of the stars than rotational modulation.

By the same argument, asymmetries in the observed eclipse profiles betray a change in brightness of the uneclipsed plasma, spatial inhomogeneity in coronal emission, optically thick absorbing material, or a mixture of these. Based on the eclipses

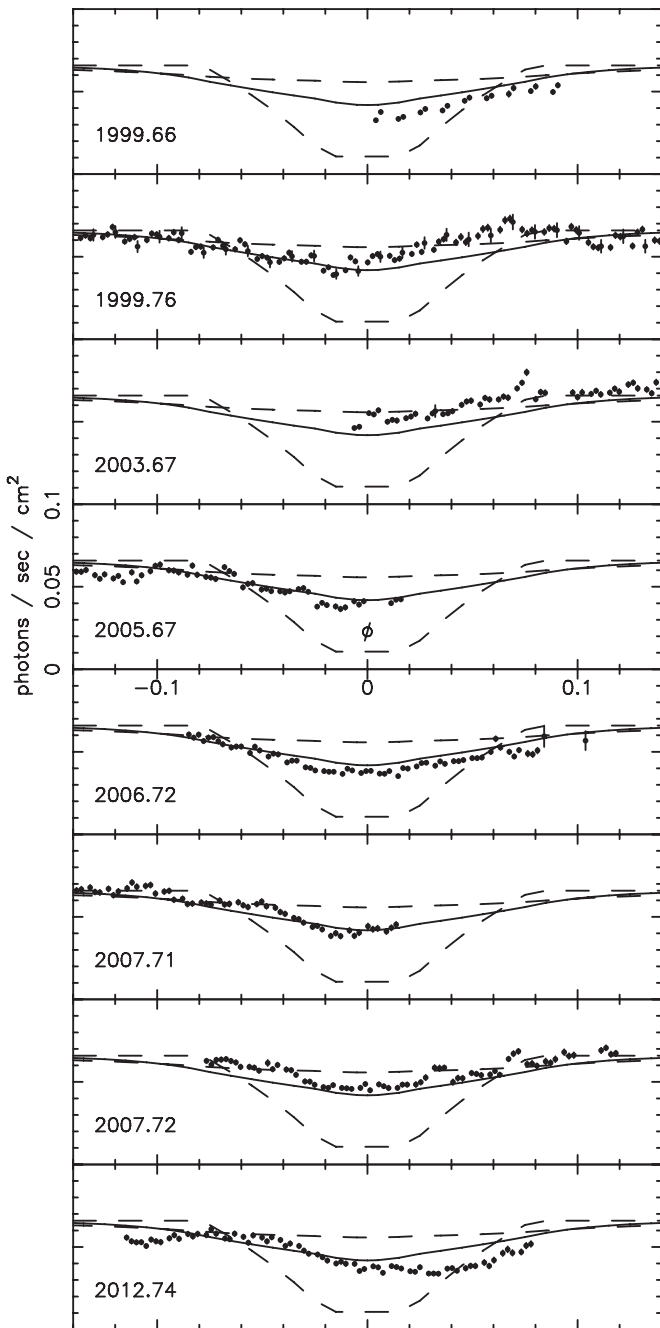


**Figure 8.** *Chandra* HRC X-ray light curves of AR Lac for data during primary eclipse that are uncontaminated by obvious flaring. Model light curves for our “best-fit” model are also shown ( $h_K = h_G = 1.3 R_\odot$ ,  $b_K = 0.44$ ; see Table 4 for a full summary of fit results), together with those for secondary coronal scale heights of  $h_K = h_G = 0$  (the deep dashed profile) and  $h_K = h_G = 2.5 R_\odot$  (the shallow dashed profile).

observed by the *Chandra* HRC, we can point to the following epochs that have essentially full eclipse coverage but asymmetric eclipse profiles: 1999.76, whose eclipse appears narrow with an early egress; 2007.72, whose eclipse also appears narrower than spherical model predictions with a late ingress; and 2012.74, whose eclipse appears broadened with egress shifted to later times.

Narrow eclipses point to less emission from the stellar limb and might be associated with intrabinary emission located between the two stars, as has been inferred in the case in previous work. Siarkowski et al. (1996) applied an iterative deconvolution

technique described by Siarkowski (1992) to *ASCA* observations in 1993 June covering slightly more than one orbital cycle. Unlike the observations presented here, secondary eclipse did appear to be present in those data, and the reconstruction of Siarkowski et al. (1996) concluded that the emission was dominated by coronal structures located between the two binary stars. We again note that this reconstruction was based on only one orbital phase, however, and it is likely that the details of the deduced spatial extent of the emission are a spurious manifestation of a sort of time-variable emission afflicting the *Chandra* data as discussed above. We therefore temper interpretation of this reconstruction with some degree of caution, although it is also notable that in this case there is an element of support for the deduced intrabinary emission from optical surface features and from Mg II line profiles of enhanced Mg II emission likely associated with extended structures co-rotating with the K star and close to the system center of mass (Pagano et al. 2001).

It is likely that coronal emission is associated with surface spots found from photometric modulation. Lanza et al. (1998) found that the spatial association between photospheric spots revealed by optical photometry and chromospheric and coronal plages as detected in the UV (e.g., Pagano et al. 2001) and the intrabinary emission deduced in X-rays by Siarkowski et al. (1996) is significant for a large active region inferred around the substellar point on the secondary and is suggested also for smaller starspots on both components. The large spots on RS CVn-type binaries, including AR Lac, appear to be fairly stable, but migrate in phase over time. On AR Lac, they are only easily discernible on the larger and optically brighter K secondary star from optical photometry and have been modeled by two large spots (e.g., Rodono et al. 1986; Lanza et al. 1998; Siviero et al. 2006). The migration rate of the spots was found to be  $0.4 \text{ period yr}^{-1}$  for data obtained in the years 1978–1981 (Rodono et al. 1986) and  $0.55 \text{ period yr}^{-1}$  for 2000–2005. Other spot activity on top of this pattern appears to be more irregular, with Siviero et al. (2006) noting that the light curve shaped by spots does not repeat cycle after cycle. Based on this spot behavior, we would not expect the X-ray morphology to be stable over long periods of time, and it is perhaps not surprising that we do not find evidence for the strong intrabinary emission that appeared to characterize the 1993 *ASCA* observations, especially if such emission depends on spot activity on both stars being concentrated on the opposing hemispheres.

Proceeding with the assumption that our simple three-parameter spherically symmetric models give a reasonable average approximation to what is more likely a distribution of discrete regions of varying brightness over the stars, we find the G star coronal scale height from Section 4.1 to be about  $1.3 R_\odot$ , or in terms of the G star radius, about  $0.86 R_*$ . This is considerably larger than the coronal scale height on the Sun, whose typical loop lengths extend to heights of  $0.04\text{--}0.4 R_\odot$  (e.g., Aschwanden 2011). This observed loop scale height also corresponds to the pressure scale height  $h_\odot = 2kT_e/\mu m_H g$ : for an active solar coronal temperature of typically about  $T_e = 2 \times 10^6 \text{ K}$  and with  $m_H$  being the proton mass,  $h_\odot = 0.2 R_\odot$ . A larger scale height for the AR Lac corone is expected naively because of lower surface gravities and higher coronal temperatures. For the G primary, the surface gravity is about half the solar value, while the typical coronal temperature is  $T_e \sim 10^7 \text{ K}$ , or five times higher than the solar corona. The scale height is then about 10 times larger or  $\sim 2 R_\odot$ . This is approximately compatible with our observations. The surface gravity of the K component is a

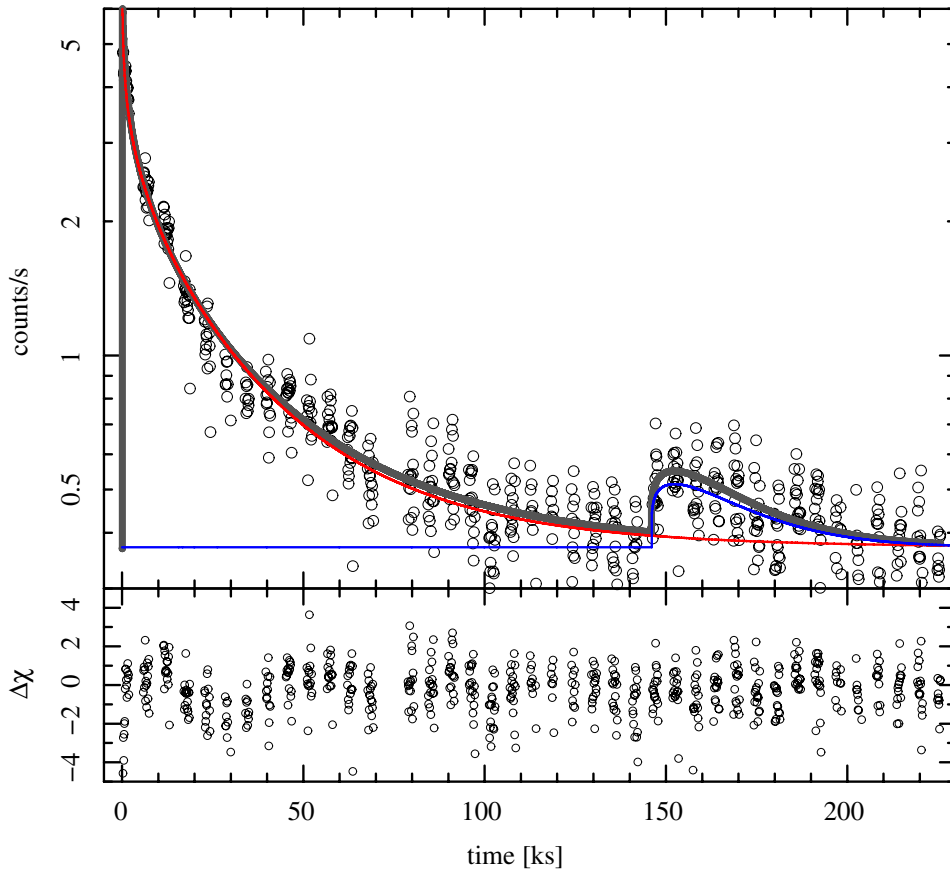


**Figure 9.** *EUVE* DS light curve, binned on 100 s intervals, and best-fit Weibull distribution model and residuals for the large flare of 2000 September 14–18. The gray curve represents the overall model, while the red and blue curves illustrate the models for the large and smaller flares, respectively.

(A color version of this figure is available in the online journal.)

factor of three lower still, and the hydrostatic scale height is about  $6 R_{\odot}$ .

The coronal scale height we find from direct geometrical eclipses is considerably larger than the  $0.05 R_{\star}$  height inferred from *EUVE* spectra for “hot” loops with temperatures in excess of  $10^7$  K by Griffiths (1999; see also Griffiths & Jordan 1998), and only slightly more consistent with their finding of  $0.15 R_{\star}$  for cooler loops with temperatures less than  $10^7$  K. Their estimates are based on energy balance models that are somewhat dependent on the adopted gas pressure. Pagano et al. (2001) found that eclipses of the K component by the G star in the light of Mg II lines were wider than the simple photospheric geometrical prediction, pointing to a significant extension of the Mg II emitting gas above the stellar surface. Our failure to detect the eclipse of the K star in X-rays points to an extended corona, as might be expected from the greater scale height, although formally we cannot provide firm observational constraints on this.

More direct measures of coronal scale height on RS CVn-type binaries are difficult to obtain. Testa et al. (2004b) used a detection of resonance scattering in lines of O VIII and Ne IX in the coronae of II Peg and IM Peg to infer small scale heights of only a few percent or less of the stellar radius. Since such scattering was not common among the spectra they investigated, it is possible that during those particular observations the visible hemisphere emission was dominated by a bright active region core. Flare scale heights based on Fe K $\alpha$  photospheric fluorescence emission of  $\lesssim 0.15 R_{\star}$  ( $0.5 R_{\odot}$ ) on II Peg and  $\lesssim 0.3 R_{\star}$  ( $4 R_{\odot}$ ) on the active K giant HR 9024 by

Ercolano et al. (2008) and Testa et al. (2008), respectively, are more consistent with our geometrical coronal heights. Eclipsed flares have been observed twice on Algol (B8 V + K2 III), whose optical secondary is similar to the evolved components of RS CVn-type binaries. The inferred heights of flaring loops are  $\lesssim 0.6 R_{\star}$  ( $2.1 R_{\odot}$ ) (Schmitt & Favata 1999) and  $\sim 0.1 R_{\star}$  ( $0.35 R_{\odot}$ ) (Schmitt et al. 2003); see also Sanz-Forcada et al. (2007). Our inference of scale height on AR Lac is then similar to other geometrical results for similar RS CVn-like stars.

## 6. X-RAYS FROM AR Lac THROUGH TIME

The HRC-I and HRC-S light curves as a function of time, in units of  $\text{erg cm}^{-2} \text{s}^{-1}$ , are illustrated in Figure 10 in the context of the fluxes observed by previous X-ray missions, beginning with *Einstein* observations in 1980 June 14 about 33 yr ago. The *Chandra* data were filtered to only include data in the phase range 0.2–0.8, outside of primary eclipse, but flares have been retained. Flux levels and uncertainties for other missions are summarized in Table 5 and were based on count rates essentially determined by eye from figures in the relevant publications in which the data have appeared. These count rates were converted to flux in the 0.5–5 keV band by folding an AR Lac spectral model through the appropriate effective area curve obtained from the Portable Interactive Multi-Mission Simulator database.<sup>5</sup> The AR Lac model was the same as that described in Section 3.1. We also performed sensitivity tests by changing

<sup>5</sup> <http://heasarc.nasa.gov/docs/software/tools/pimms.html>

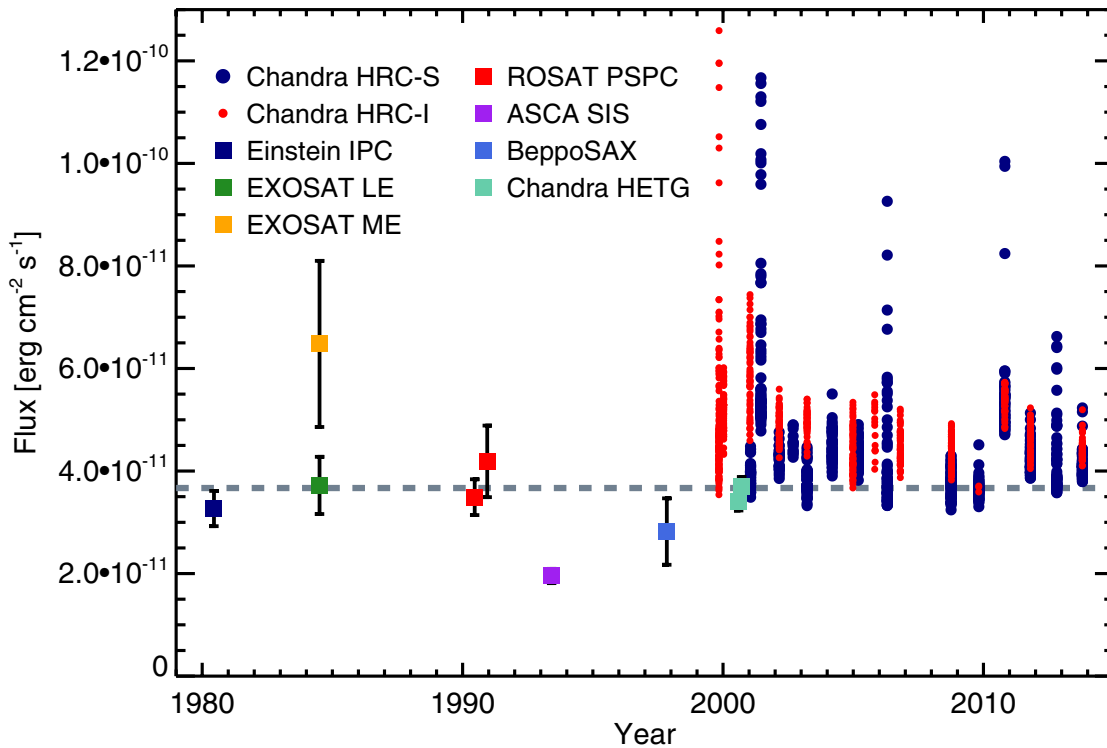


**Figure 10.** *Chandra* HRC-S and HRC-I X-ray light curves in the context of earlier X-ray observations of AR Lac. HRC data have been filtered to exclude primary eclipse within the phase range 0.8–1.2, but flares have been retained. Earlier observations are summarized in Table 5. The dashed horizontal line represents the mean of the observations prior to *Chandra*. The mean quiescent X-ray flux from AR Lac has remained consistently at  $3.7 \times 10^{-11}$  erg cm $^{-2}$  s $^{-1}$ , to within about 10% if the ASCA SIS point is discarded, for the past 33 yr.

(A color version of this figure is available in the online journal.)

**Table 5**  
Multi-decade Observation Information

Instrument	Date	Rate <sup>a</sup> (counts s $^{-1}$ )	Flux <sup>b</sup> (erg cm $^{-2}$ s $^{-1}$ )
<i>Einstein</i> IPC	1980 Jun 14	$1.9 \pm 0.2^c$	$3.2 \times 10^{-11}$
<i>EXOSAT</i> LE	1984 Jul 4	$0.2 \pm 0.02^d$	$2.5 \times 10^{-11}$
<i>EXOSAT</i> ME	1984 Jul 4	$0.5 \pm 0.15^d$	$2.4 \times 10^{-11}$
<i>ROSAT</i> PSPC	1990 Jun 18	$5.0 \pm 0.5^e$	$3.2 \times 10^{-11}$
<i>ROSAT</i> PSPC	1990 Dec 11	$6.0 \pm 1.0^f$	$3.9 \times 10^{-11}$
<i>ASCA</i> SIS	1993 Jun 2	$1.05 \pm 0.15^g$	$2.0 \times 10^{-11}$
<i>Beppo-SAX</i>	1997 Nov 2,9	...	$2.8 \times 10^{-11h}$
<i>Chandra</i> HETG	2000 Sep 11	$1.0 \pm 0.05^i$	$3.4 \times 10^{-11i}$
<i>Chandra</i> HETG	2000 Sep 17	$1.0 \pm 0.05^i$	$3.8 \times 10^{-11i}$

**Notes.**

<sup>a</sup> Count rates listed are our own assessments of the quiescent rate outside of eclipses based on data presented in the references indicated.

<sup>b</sup> Except where noted, fluxes are based on the spectral model described in Section 3.1 and refer to the 0.5–5.0 keV bandpass.

<sup>c</sup> Walter et al. (1983).

<sup>d</sup> White et al. (1990); count rate refers to LE1 only.

<sup>e</sup> Ottmann et al. (1993).

<sup>f</sup> Schmitt (1992).

<sup>g</sup> White et al. (1994); count rate refers to a single SIS.

<sup>h</sup> Rodonò et al. (1999); flux taken directly from their Table 2 with uncertainty based on light-curve variations in their Figure 2.

<sup>i</sup> Huenemoerder et al. (2003); flux determined by direct integration of HETG spectrum.

the spectral model to the two-temperature best-fit model for the out-of-eclipse ASCA observations analyzed by Singh et al. (1996), and by halving the abundances of metals. In all cases, the conversions from counts to flux changed by less than 10%.

The base flux level of AR Lac—i.e., not considering flares—has been remarkably constant over the 13 yr covered by *Chandra* and varies by only 10% or so. Looking back further, over the 33 yr of X-ray observations, the same base level is seen with only the ASCA observations from 1993 appearing significantly fainter than in the *Chandra* era by about 45%. The 1984 *EXOSAT* ME observation is only marginally consistent, but the instrument was only sensitive to X-ray energies above 1 keV and the derived flux is very sensitive to the adopted hot emission measure (see, e.g., White et al. 1990). The mean of the fluxes for the earlier missions,  $3.7 \times 10^{-11}$  erg cm $^{-2}$  s $^{-1}$ , is in good agreement with the *Chandra* measurements, while we also note that absolute calibration uncertainties of earlier missions could account for systematic differences at the 10% or so level.

There is no evidence for any significant cyclic modulation, at least on the timescales covered by our observations. The orbital period of AR Lac has long been known to exhibit an oscillatory behavior with a reported period of 35–50 yr on top of a steady decline (Hall & Kreiner 1980; van Buren 1986; Kim 1991; Jetsu et al. 1997; Lanza et al. 1998; Qian et al. 1999; Lu et al. 2012). The origin of the oscillatory component remains uncertain, though Lanza et al. (1998) noted a possible relation with a  $\sim 17$  yr surface spot cycle attributed to the K star and suggested that the period variation could be due to the Applegate (1992) mechanism that is driven by a magnetic cycle. Since the G star appears to dominate the coronal emission, its cyclic behavior would appear to be more relevant to this study than cycles on the K star. The long baseline of the X-ray data presented here cannot rule out magnetic cycles, but any such cycle with a period of 17 or 35 yr has very little influence on the X-ray coronal energy output.

Kashyap & Drake (1999) investigated the X-ray emission of active binary stars observed at various epochs by the *Einstein* and *ROSAT* satellites and found that fluxes differed by 30%–40% or so on average between different epochs. That study could only examine data averaged over whole observations, or in the case of *ROSAT*, averaged over the all-sky survey, and so any flares would be implicitly included in the averages. Figure 10 demonstrates that typical base-level emission variations are likely to be significantly smaller. Relatively constant basal emission over decade timescales also appears to characterize the young K1 dwarf AB Dor (Lalitha & Schmitt 2013), despite evidence for an optical cycle, and the low-mass flare star VB8 (Drake et al. 1996) and appears to be a general characteristic of very active stars.

## 7. SUMMARY AND CONCLUSIONS

We have analyzed an extensive set of *Chandra* HRC observations of the eclipsing RS CVn-type binary AR Lac obtained over a 13 yr period and combined these data with observations by *EUVE*, *ASCA*, *ROSAT*, *EXOSAT*, and *Einstein* that go back to 1980. We find the quiescent base level coronal emission to be remarkably constant, with typical variations of 15% or less over a period of 33 yr. Multi-orbit *Chandra* and *EUVE* observations indicate that stochastic variability likely dominates rotationally modulated variability on orbital timescales. Consequently, reconstructions of the spatial distribution of emitting plasma should be treated with caution. Primary eclipses, when the more compact G2 IV component lies behind the K0 subgiant, are regularly detected, but obvious secondary eclipses are absent. Spherically symmetric coronal models fitted to the *Chandra* and *EUVE* light curves cannot constrain the K star coronal scale height, but indicate a coronal scale height on the G component of  $1.3 R_{\odot}$ , or  $0.86 R_{*}$ , and that the G star dominates the emission by a factor of 2–5.

J.J.D., V.K., P.R., and B.J.W. were funded by NASA contract NAS8-03060 to the Chandra X-ray Center (CXC) and thank the CXC director, H. Tananbaum, and the CXC science team for advice and support. D.P.H. was supported by Smithsonian Astrophysical Observatory contract SV3-73016 to MIT for Support of the Chandra X-Ray Center.

## REFERENCES

- Agrawal, P. C., & Vaidya, J. 1988, *MNRAS*, **235**, 239  
 Applegate, J. H. 1992, *ApJ*, **385**, 621  
 Aschwanden, M. J. 2011, *LRSP*, **8**, 5  
 Audard, M., Güdel, M., & Mewe, R. 2001, *A&A*, **365**, L318  
 Bowyer, S., & Malina, R. F. 1991, *AdSpR*, **11**, 205  
 Chambliss, C. R. 1976, *PASP*, **88**, 762  
 Christian, D. J., Drake, J. J., Patterer, R. J., Vedder, P. W., & Bowyer, S. 1996, *AJ*, **112**, 751  
 Culhane, J. L., White, N. E., Parmar, A. N., & Shafer, R. A. 1990, *MNRAS*, **243**, 424  
 Dempsey, R. C., Linsky, J. L., Schmitt, J. H. M. M., & Fleming, T. A. 1993, *ApJ*, **413**, 333  
 den Herder, J. W., Brinkman, A. C., Kahn, S. M., et al. 2001, *A&A*, **365**, L7  
 Drake, J. J. 1999, *ApJS*, **122**, 269  
 Drake, J. J., Brown, A., Patterer, R. J., et al. 1994, *ApJL*, **421**, L43  
 Drake, J. J., Peres, G., Orlando, S., Laming, J. M., & Maggio, A. 2000, *ApJ*, **545**, 1074  
 Drake, J. J., Stern, R. A., Stringfellow, G., et al. 1996, *ApJ*, **469**, 828  
 Drake, S. A., Simon, T., & Linsky, J. L. 1992, *ApJS*, **82**, 311  
 Ercolano, B., Drake, J. J., Reale, F., Testa, P., & Miller, J. M. 2008, *ApJ*, **688**, 1315  
 Flaccio, E., Micela, G., Sciortino, S., et al. 2005, *ApJS*, **160**, 450  
 García-Alvarez, D., Barnes, J. R., Collier Cameron, A., et al. 2003, *A&A*, **402**, 1073  
 Griffiths, N. W. 1999, *ApJ*, **518**, 873  
 Griffiths, N. W., & Jordan, C. 1998, *ApJ*, **497**, 883  
 Guedel, M. 1997, *ApJL*, **480**, L121  
 Guedel, M., Schmitt, J. H. M. M., & Benz, A. O. 1995a, *A&A*, **293**, L49  
 Guedel, M., Schmitt, J. H. M. M., Benz, A. O., & Elias, N. M., II 1995b, *A&A*, **301**, 201  
 Hall, D. S. 1978, *AJ*, **83**, 1469  
 Hall, D. S., & Kreiner, J. M. 1980, *AcA*, **30**, 387  
 Huenemoerder, D. P., Canizares, C. R., Drake, J. J., & Sanz-Forcada, J. 2003, *ApJ*, **595**, 1131  
 Huenemoerder, D. P., Schulz, N. S., Testa, P., et al. 2010, *ApJ*, **723**, 1558  
 Jetsu, L., Pagano, I., Moss, D., et al. 1997, *A&A*, **326**, 698  
 Jordan, C., Ayres, T. R., Brown, A., Linsky, J. L., & Simon, T. 1987, *MNRAS*, **225**, 903  
 Kashyap, V., & Drake, J. J. 1999, *ApJ*, **524**, 988  
 Kenter, A. T., Chappell, J. H., Kraft, R. P., et al. 2000, *Proc. SPIE*, **4012**, 467  
 Kim, C.-H. 1991, *AJ*, **102**, 1784  
 Kuerster, M., Schmitt, J. H. M. M., Cutispoto, G., & Dennerl, K. 1997, *A&A*, **320**, 831  
 Lalitha, S., & Schmitt, J. H. M. M. 2013, *A&A*, **559**, A119  
 Lanza, A. F., Catalano, S., Cutispoto, G., Pagano, I., & Rodono, M. 1998, *A&A*, **339**, 309  
 Lu, Y., Xiang, F.-Y., & Shi, X.-M. 2012, *PASJ*, **64**, 84  
 Makarov, V. V. 2003, *AJ*, **126**, 1996  
 Marino, A., Micela, G., Peres, G., & Sciortino, S. 2003, *A&A*, **407**, L63  
 Marino, G., Catalano, S., Frasca, A., & Marilli, E. 1998, *IBVS*, **4599**, 1  
 Ness, J.-U., Güdel, M., Schmitt, J. H. M. M., Audard, M., & Telleschi, A. 2004, *A&A*, **427**, 667  
 Ottmann, R., Schmitt, J. H. M. M., & Kuerster, M. 1993, *ApJ*, **413**, 710  
 Owen, F. N., & Spangler, S. R. 1977, *ApJL*, **217**, L41  
 Pagano, I., Rodono, M., Linsky, J. L., et al. 2001, *A&A*, **365**, 128  
 Pallavicini, R., Golub, L., Rosner, R., et al. 1981, *ApJ*, **248**, 279  
 Pandey, J. C., & Singh, K. P. 2012, *MNRAS*, **419**, 1219  
 Popper, D. M. 1990, *AJ*, **100**, 247  
 Popper, D. M., & Ulrich, R. K. 1977, *ApJL*, **212**, L131  
 Qian, S.-B., Liu, Q.-Y., & Yang, Y.-L. 1999, *ChA&A*, **23**, 317  
 Rodono, M., Cutispoto, G., Pazzani, V., et al. 1986, *A&A*, **165**, 135  
 Rodono, M., Pagano, I., Leto, G., et al. 1999, *A&A*, **346**, 811  
 Sanz-Forcada, J., Brickhouse, N. S., & Dupree, A. K. 2003, *ApJS*, **145**, 147  
 Sanz-Forcada, J., Favata, F., & Micela, G. 2007, *A&A*, **466**, 309  
 Schmitt, J. H. M. M. 1992, *RvMA*, **5**, 188  
 Schmitt, J. H. M. M., & Favata, F. 1999, *Natur*, **401**, 44  
 Schmitt, J. H. M. M., Ness, J.-U., & Franco, G. 2003, *A&A*, **412**, 849  
 Schulz, N. S., Testa, P., Huenemoerder, D. P., Ishibashi, K., & Canizares, C. R. 2006, *ApJ*, **653**, 636  
 Siarkowski, M. 1992, *MNRAS*, **259**, 453  
 Siarkowski, M., Pres, P., Drake, S. A., White, N. E., & Singh, K. P. 1996, *ApJ*, **473**, 470  
 Singh, K. P., White, N. E., & Drake, S. A. 1996, *ApJ*, **456**, 766  
 Siviero, A., Dallaporta, S., & Munari, U. 2006, *BaltA*, **15**, 387  
 Swank, J. H., Holt, S. S., White, N. E., & Becker, R. H. 1981, *ApJ*, **246**, 208  
 Testa, P., Drake, J. J., Ercolano, B., et al. 2008, *ApJL*, **675**, L97  
 Testa, P., Drake, J. J., & Peres, G. 2004a, *ApJ*, **617**, 508  
 Testa, P., Drake, J. J., Peres, G., & DeLuca, E. E. 2004b, *ApJL*, **609**, L79  
 Testa, P., Drake, J. J., Peres, G., & Huenemoerder, D. P. 2007, *ApJ*, **665**, 1349  
 Triglilio, C., Buemi, C. S., Umana, G., et al. 2001, *A&A*, **373**, 181  
 van Buren, D. 1986, *AJ*, **92**, 136  
 Walter, F., Charles, P., & Bowyer, S. 1978, *AJ*, **83**, 1539  
 Walter, F. M. 1996, in *IAU Colloq. 152, Astrophysics in the Extreme Ultraviolet*, ed. S. Bowyer & R. F. Malina (Dordrecht: Kluwer), **129**  
 Walter, F. M., Gibson, D. M., & Basri, G. S. 1983, *ApJ*, **267**, 665  
 Weisskopf, M. C., Aldcroft, T. L., Bautz, M., et al. 2003, *ExA*, **16**, 1  
 Welsh, B. Y., Vallerger, J. V., Jelinsky, P., et al. 1989, *Proc. SPIE*, **1160**, 554  
 White, N. E., Arnaud, K., Day, C. S. R., et al. 1994, *PASJ*, **46**, L97  
 White, N. E., Shafer, R. A., Parmar, A. N., Horne, K., & Culhane, J. L. 1990, *ApJ*, **350**, 776